# AIAA 2003-0975

## Numerical simulations of wake/boundary layer interactions

Ugo Piomelli
*Department of Mechanical Engineering*
*University of Maryland, College Park, MD 20742*

Meelan M. Choudhari
*NASA Langley Research Center, Hampton, VA 23681*

Victor Ovchinnikov and Elias Balaras
*Department of Mechanical Engineering*
*University of Maryland, College Park, MD 20742*

41st Aerospace Sciences
Meeting and Exhibit
6–9 January 2003
Reno, Nevada

# Numerical simulations of wake/boundary layer interactions

Ugo Piomelli *
*Department of Mechanical Engineering*
*University of Maryland, College Park, MD 20742*

Meelan M. Choudhari †
*NASA Langley Research Center, Hampton, VA 23681*

Victor Ovchinnikov ‡and Elias Balaras §
*Department of Mechanical Engineering*
*University of Maryland, College Park, MD 20742*

**Direct and large-eddy simulations of the interaction between the wake of a circular cylinder and a flat-plate boundary layer are conducted. Two Reynolds numbers are examined. The simulations indicate that at the lower Reynolds number the boundary layer is buffeted by the unsteady Kármán vortex street shed by the cylinder. The fluctuations, however, cannot be self-sustained due to the low Reynolds-number, and the flow does not reach a turbulent state within the computational domain. In contrast, in the higher Reynolds-number case, boundary-layer fluctuations persist after the wake has decayed (due, in part, to the higher values of the local Reynolds number $Re_\theta$ achieved in this case); some evidence could be observed that a self-sustaining turbulence generation cycle was beginning to be established.**

## Introduction

High-lift systems have a significant impact on the overall cost and safety of aircraft. According to Meredith,[1] a 1% improvement in the maximum lift coefficient (or lift-to-drag ratio) could translate into an increased payload of 14 to 22 passengers on a large twin-engine transport. An optimal aerodynamic design of a multi-airfoil high-lift configuration requires careful consideration of both inviscid and viscous flow phenomena. In particular, laminar-to-turbulent transition is a crucial issue for ground-to-flight scaling of high-lift flow fields.

Either of the familiar transition mechanisms for a single-element configuration are also relevant to transition over a multi-airfoil configuration: those associated with streamwise instabilities in the form of Tollmien-Schlichting or Rayleigh modes, cross-flow and attachment line instabilities, and leading-edge contamination—a form of subcritical (*i.e.*, bypass) transition. However, a unique transition mechanism in the case of multi-element flow-fields involves the boundary-layer contamination due to unsteady wake(s) from the preceding element(s) and/or additional forms of vortical disturbances originating from the separated, cove flow underneath an upstream element (Fig. 1). While the "single-element" class of transition mechanisms have been widely studied in the literature, the wake-contamination issue has received little scrutiny thus far and is the focus of this paper.

Interactions between turbulent wakes and boundary layers have been the subject of much study. Most of the investigations, however, concentrated on the unsteady case that occurs, for instance, in turbomachinery, when the wake of an upstream blade impinges on a downstream blade; the unsteadiness of the impingement region plays an important role in the dynamics of the flow. Fewer studies can be found of the steady case. Squire[2] summarizes much of the investigations conducted prior to 1989. Particularly important is the work by Zhou and Squire[3] who examined the interaction between the wake of an airfoil and a flat plate. They found that, a region in which the wake and boundary layer are separated by a potential core is followed by a merging zone, in which the velocity profile in the outer layer is substantially different from that in a regular flat-plate boundary layer. They also observed that the position of zero Reynolds shear stress

**Fig. 1 Sketch of the wake/boundary-layer interactions on an airfoil.**

*Professor, AIAA Senior Member
†Senior Research Scientist
‡Graduate Research Assistant
§Assistant Professor

and that of zero mean-velocity gradient do not coincide, an important issue for eddy-viscosity turbulent models.

Recently, Kyriakides and co-workers[4–6] performed a series of experiments involving the interaction between the wake of a large-aspect-ratio circular cylinder and a flat-plate boundary layer. These experiments spanned a range of Reynolds numbers and cylinder diameters, including cases in which the wake still contained coherent eddies in the interaction region (i.e., the so called case of "strong interaction") and others in which the interaction took place sufficiently far downstream of the cylinder, such that the spanwise rollers had decayed significantly (i.e., "weak interaction" cases). While they provided measurements for a range of Reynolds numbers, Kyriakides *et al.*[4–6] did not clarify how transition could occur (and turbulence could be self-sustained) at the lowest Reynolds numbers examined.

Due to the tremendous challenges inherent in a high-fidelity simulation of the wake-contamination problem, we also choose to study a simple, building-block problem, namely that of interaction between a flat-plate boundary layer and the wake of a circular cylinder that is placed above the flat plate. This model problem provides a reasonable balance between simplicity (two-dimensional geometry involving a combination of two canonical flow fields) and the numerical challenges of a complex-geometry simulation including the wake generator and a boundary layer. Simultaneously, it allows one to investigate a range of issues, such as the effect of Reynolds number and the role of the spacing between the cylinder and plate (which allows one to traverse the continuous range from strong wake interactions to weak interactions that are analogous to conventional free-stream turbulence). Effects of flow three-dimensionality and/or transverse pressure gradients (which lead to curved wakes) may also be captured, if necessary, by modifying the free-stream boundary conditions. Most significantly, a limited amount of experimental data is available for a range of flow and geometry parameters.[4–6]

In the present paper we report the initial results from a series of numerical experiments designed to study the physical phenomena underlying wake/boundary-layer interactions of this type. The first stage of this investigation involves the study of the strong interaction case, with the specific aims to clarify some issues left unresolved by the experimental studies, and to document the flow field in detail. In particular, we will focus on the issue of transition mechanisms at low Reynolds number, which was only partially addressed in the experiment. Thus, we choose to examine low Reynolds-number cases first, before attempting the more challenging simulations at higher Reynolds numbers. Future work will focus on the weak interaction case, as well as other shapes of wake generators.

Herein, we analyze direct and large-eddy simulations of two cases studied by Kyriakides *et al.*,[4] having the same geometry but different Reynolds numbers, which lead to different responses of the boundary layer to the unsteady wake in the free stream. Despite the simplicity of the geometrical configuration, conducting DNS and LES of the above problem is a challenge for most numerical methods available today. In the present study we model the effect of the cylinder using an "immersed boundary" formulation.[11] This approach enables one to use codes in Cartesian coordinates, which present significant advantages, in terms of speed, accuracy and flexibility, over codes that employ body-fitted grids.

The outline of the paper is as follows: the numerical formulation of the problem including the geometry of the cylinder-plate configuration are described first. Then, the numerical methodology will be presented. We will then present validation of the numerical tool in the context of two building-block problems relevant to the flow configuration of interest; results of the simulations will be compared with numerical and experimental data. Results for the wake/boundary-layer interaction are discussed next. Finally, conclusions and recommendations for future work are presented.

## Problem formulation

In this work we present both DNS and LES results. In the DNS case, the Navier-Stokes equations are solved:

$$\frac{\partial u_j}{\partial x_j} = 0, \tag{1}$$

$$\frac{\partial u_i}{\partial t} + \frac{\partial}{\partial x_j}\left(u_j u_i\right) = -\frac{1}{\rho}\frac{\partial p}{\partial x_i} + \nu \nabla^2 u_i + f_i. \tag{2}$$

For the LES, we use the filtered equations of conservation of mass and momentum

$$\frac{\partial \overline{u}_j}{\partial x_j} = 0, \tag{3}$$

$$\frac{\partial \overline{u}_i}{\partial t} + \frac{\partial}{\partial x_j}\left(\overline{u}_j \overline{u}_i\right) = -\frac{\partial \overline{p}}{\partial x_i} + \frac{1}{Re_\tau}\nabla^2 \overline{u}_i - \frac{\partial \tau_{ji}}{\partial x_j} + \overline{f}_i \tag{4}$$

(where the over-bar denotes filtered variables and the effect of the subgrid scales appears through the SGS stresses $\tau_{ij} = \overline{u_i u_j} - \overline{u}_i \overline{u}_j$); $f_i$ and $\overline{f}_i$ are the body forces used in the immersed-boundary method to enforce the no-slip conditions on the body.

For both DNS and LES, the equations of motion are solved numerically using a second-order accurate finite-difference method on a staggered grid. In all cases the grid is uniform in the spanwise direction $y$, stretched in the streamwise and normal ones ($x$ and $z$, respectively) to allow accurate resolution of

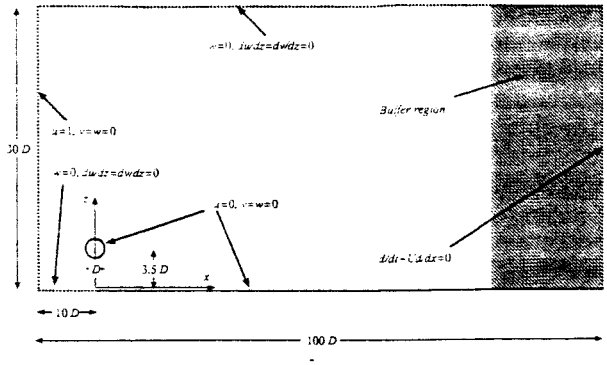


**Fig. 2 Sketch of the computational configuration and boundary conditions. The drawing is not to scale.**

the boundary layer and of the shear layers emanating from the cylinder. The discretized equations are integrated in time using an explicit fractional time-step method,[7,8] in which all terms are advanced in time using the Adams-Bashforth method. The Poisson equation is then solved using a direct solver, and the velocity is corrected to make the field solenoidal. For the LES, the SGS stresses are parameterized using the Lagrangian Dynamic eddy-viscosity model,[9] which has been shown to give accurate results in transitional flows.

The effect of the cylinder, which does not coincide with the grid lines, is introduced using an "immersed boundary" formulation. In our implementation the enforcement of non-slip boundary conditions on the cylinder surface is performed using a method similar to the the "discrete forcing" approach introduced by Mohd-Yusof[10] and Fadlun *et al.*[11] With this approach, the solution is reconstructed at the grid nodes near the boundary to ensure satisfaction of the no-slip conditions. While Mohd-Yusof[10] and Fadlun *et al.*[11] used a simple one-dimensional reconstruction scheme, in the present study we employ a multidimensional procedure proposed by Balaras,[13] in which the solution is reconstructed along the line normal to the interface.

The code is parallelized using MPI message-passing routines; the parallelization is performed by domain-decomposition process. Except for the Poisson solver, the computational domain is divided into a number subdomains in the $z$ directions, each of which is assigned to one processor. In the Poisson solver, after the velocity divergence is Fourier-transformed in the spanwise directions, each processor is responsible for a set of spanwise modes.

We applied the following boundary conditions (see Fig. 2):

1. At the inlet, a uniform velocity in the $x$ direction was assigned.

2. At the outlet, radiative boundary conditions[17] were given. Furthermore, over the last 30% of the domain (which contains only 5% of the grid points) the mesh was stretched very significantly, to generate a buffer layer in which the equations are effectively parabolized because of the large aspect ratio of the cells.

3. In the spanwise direction, $y$, periodic conditions were used.

4. In the freestream, we used a slip-wall boundary condition.

5. On the cylinder surface, no-slip conditions were enforced using the methodology described in Balaras.[13] The cylinder was placed at a height of $3.5D$ above the nominal leading-edge of the plate.

6. On the $z = 0$ surface, we used free-slip conditions ($w = 0$, $\partial u/\partial z = \partial v/\partial z = 0$) ahead of the plate, and no-slip conditions ($u_i = 0$) on the plate. A sharp transition between free-slip and no-slip was found to generate numerical oscillations; therefore, a hyperbolic tangent profile was used to merge free-slip and no-slip conditions in a smooth fashion. As a result, the origin of the boundary layer on the plate cannot be determined precisely; in the present calculations, the virtual origin of the boundary layer appears to be approximately $1.5D$ upstream of the actual leading edge.

Two calculations were carried out, corresponding to cases 1 and 2 of Kyriakides *et al.*[4] The geometry for the two cases was the same, but the free-stream velocity was varied to obtain Reynolds numbers $Re_D$ equal to 385 and 1,155, respectively. The definition of the Reynolds number is based on the free-stream velocity and cylinder diameter. The extent of the computational domain in the streamwise and wall-normal directions was $100D$ and $30D$, as shown in Fig. 1. The spanwise width of the domain was $2\pi D$ wide, a length sufficient to include several rib vortices, and to resolve the three-dimensional structures in the cylinder wake.

## Code validation

The code used in this paper has been extensively validated for a variety of turbulent[14,15] and re-laminarizing[16] flows. The "immersed boundary" formulation which is used to enforce non-slip boundary conditions on the cylinders surface, has also been extensively tested in the context of the present code.[13] In particular, a series of three-dimensional computations were conducted of the flow around a circular cylinder at $Re_D = 300$. These involved a total number of grid points ranging from $1.5 \times 10^6$ to $4.7 \times 10^6$. The agreement of the results with reference computations using boundary fitted coordinates demonstrated the accuracy of the method. Details on the above computations can be found in Balaras.[13]

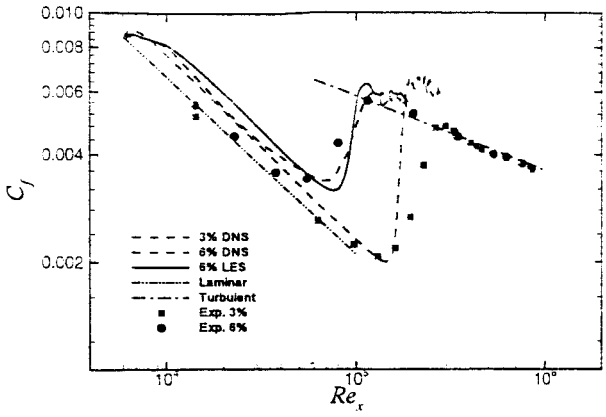


**Fig. 3 Streamwise development of the skin-friction coefficient $C_f$.**

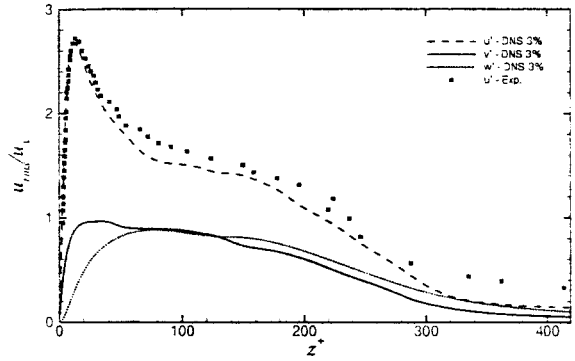


**Fig. 4 Profiles of the streamwise turbulence intensity, $u_{rms}$.**

The grid required for accurate simulations of bypass transition needs to be determined carefully. To this end, we performed simulations of bypass transition on a flat plate due to free-stream turbulence. We used the setup adopted by Voke and Yang.[18] The calculation was started at the streamwise location $Re_x \simeq 6,000$; the inflow condition consisted of a Blasius boundary layer, on which turbulent fluctuations were added. The fluctuations were obtained from a separate calculation of spatially developing homogeneous isotropic turbulence. To avoid introducing excessively large fluctuations near the wall, the turbulent fluctuations were windowed in such a way that they vanished at $2\delta_o/3$ (where $\delta_o$ is the inflow boundary-layer thickness). Two cases were run, with a 3% and a 6% freestream turbulence amplitude, to match the calculations[18] and the experimental data.[19] The description of the inflow conditions both for the experiment and the LES calculations was not, however, detailed enough to allow us to reproduce exactly the experimental setup.

We performed DNS of both cases. For the 3% case, we $350 \times 96 \times 96$ points to simulate a domain that had dimensions $714\delta_o \times 32\delta_o \times 48\delta_o$; For the 6% case, 550 points were used in the streamwise direction to discretize a box that was $476\delta_o$ long. The mesh was uniform in the spanwise direction, and stretched in the $x$ and $z$ directions. In the transition region, the grid size was approximately $\Delta x = 0.2\delta$, $\Delta y = 0.08\delta$; at least 40 points were used to discretize the local boundary layer thickness, $\delta$. For the LES of the 6% case, $300 \times 64 \times 96$ points were used, resulting in coarser resolution in $x$ and $y$: $\Delta x = 0.4\delta$, $\Delta y = 0.1\delta$.

The streamwise development of the skin-friction coefficient $C_f = 2\tau_w/\rho U_\infty^2$ is shown in Fig. 3. One can observe a higher skin-friction coefficient in the laminar region, due to the perturbation introduced at the inflow, which generates a pressure disturbance that propagates well inside the boundary layer and distorts the mean-velocity profile in the near-wall region. It was verified that, in the absence of inflow disturbances, the Blasius profile was recovered. The slope of the skin-friction coefficient distribution is, however correct. The transition begins at the correct location for both values of the freestream turbulence intensity, and the extent of the transition region is also predicted with reasonable accuracy. The LES calculation predicts the a slightly delayed beginning of the rise of $C_f$, and a somewhat more rapid transition; the results are, however, in reasonable agreement with the DNS and the experiments. In Fig. 4 the distributions or the r.m.s. turbulence intensities at $Re_x = 290,000$ (for the 3% freestream turbulence case) are compared with the experimental data of Roach and Brierley.[19] The agreement is again satisfactory, given the uncertainty in the inflow condition generation.

Finally, a grid refinement study was carried out on the real geometry. Two grids were tested, a coarse one that used $576 \times 48 \times 192$ grid points and a medium one with $864 \times 72 \times 288$ points. Calculations on a finer grid with $1056 \times 128 \times 384$ points are currently underway. The coarse grid was similar to the one that gave grid-converged results in the cylinder calculation. Figure 5 shows the mean velocity profile and the trace of the Reynolds stresses $q^2 = \langle u_i' u_i' \rangle$ (throughout this paper $\langle \cdot \rangle$ represents a long-time average, and $f' = f - \langle f \rangle$ is the fluctuating component of $f$) at three locations downstream of the cylinder. Very little difference can be observed between the coarse and medium grids for the mean velocity profiles; the coarse resolution of the wake and boundary layer results in some difference in $q^2$ between the coarse and medium meshes, but the agreement is altogether satisfactory. In the following, the medium grid results will be presented.

Notice that the resolution of the boundary layer in the medium grid compares favorably with the bypass transition case mentioned above. In the transition region, the grid spacing was $\Delta x = 0.07\delta$, $\Delta y = 0.06\delta$ (where $\delta$ is the local boundary layer thickness). At least 80 points were used to discretize the boundary-layer thickness.

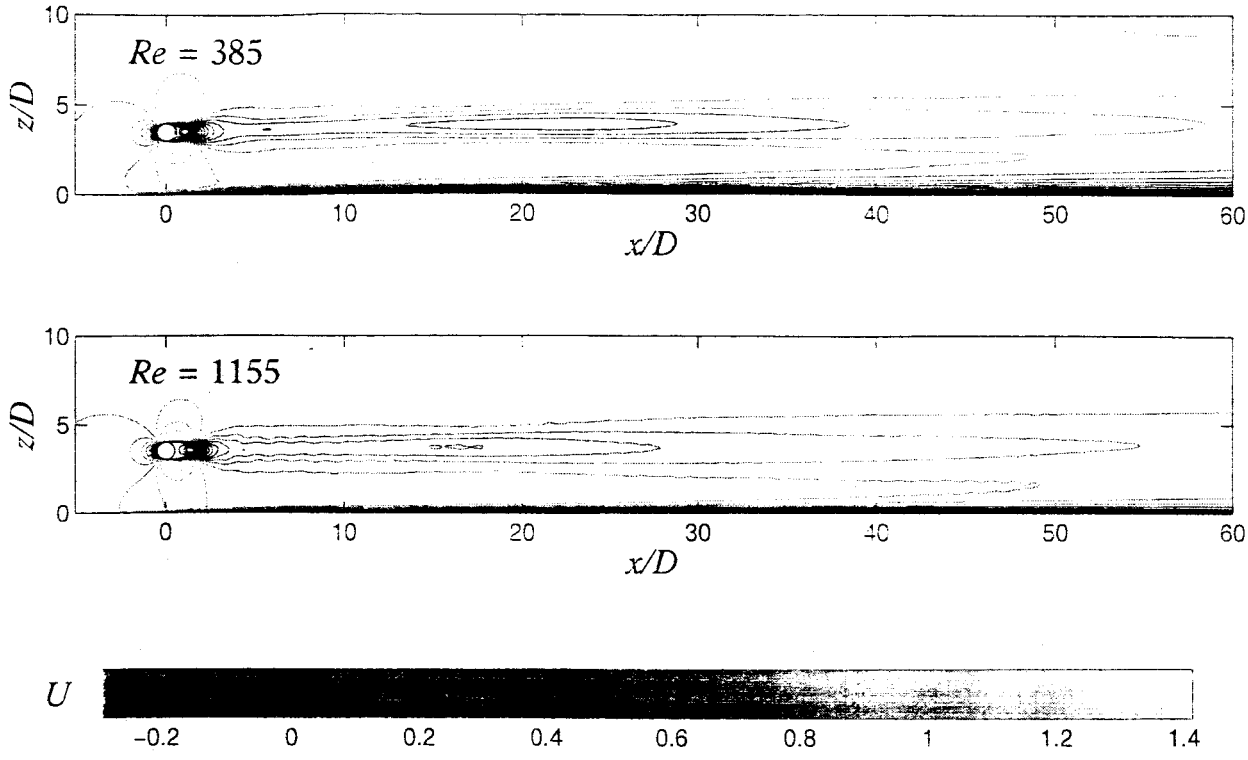


**Fig. 6 Mean velocity contours.** —— $Re_D = 385$; --- $Re_D = 1,155$.

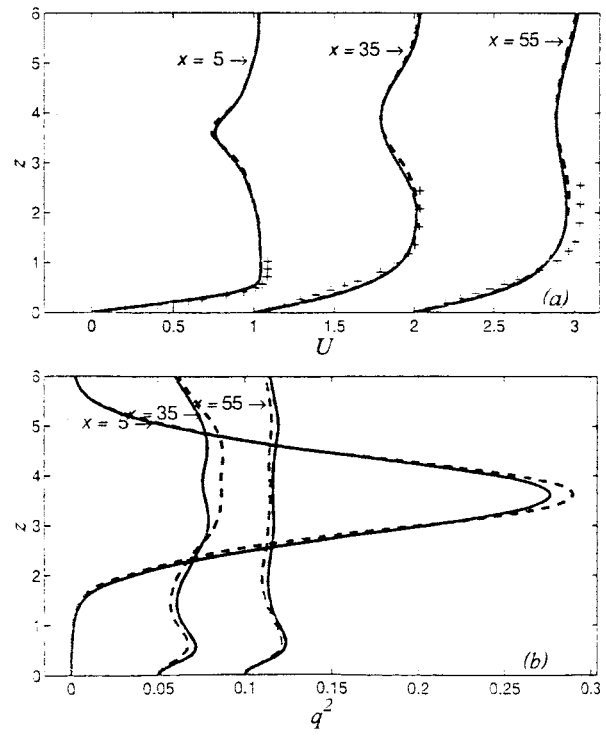


**Fig. 5 (a) Mean velocity profiles and (b) profiles of $q^2$, $Re_D = 385$.** —— $576 \times 48 \times 192$ **grid;** --- $864 \times 72 \times 288$; × **Blasius solution.**

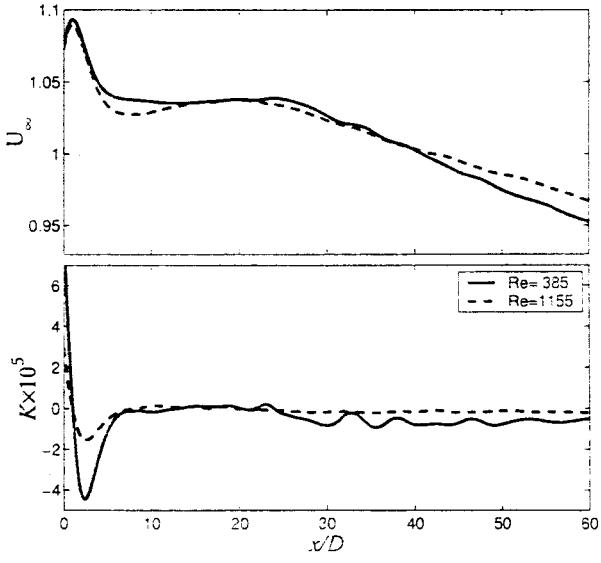


**Fig. 7 Streamwise development of: (a) the velocity at the edge of the boundary layer; (b) the acceleration parameter $K$.**

## Results and discussion

The mean-velocity contours from the wake/boundary-layer simulations at $Re_D = 385$ and $Re_D = 1,155$ are shown in Fig. 6. As expected, both the wake and the boundary layer are thinner at the higher Reynolds number. No merging is observed within the computational domain. Due to the presence of the cylinder, the boundary layer near

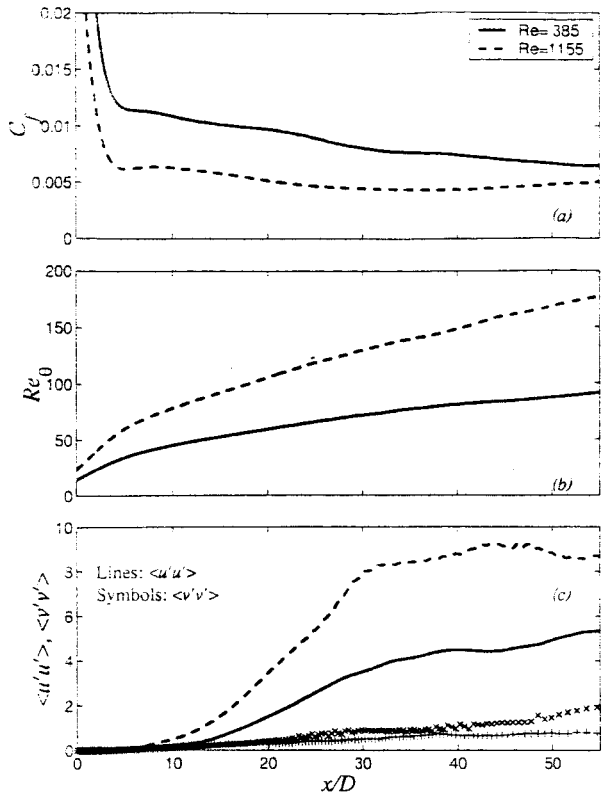


**Fig. 8 Streamwise development of statistical quantities. (a) skin friction coefficient $C_f$; (b) Reynolds number based on the momentum thickness, $Re_\theta$; (c) peak streamwise and spanwise Reynolds stresses in the boundary layer.**

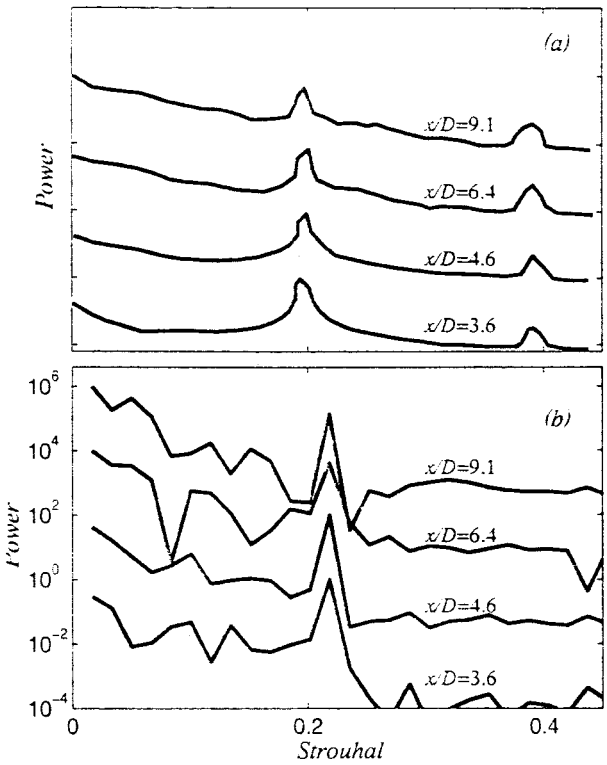


**Fig. 9 Power spectra of the streamwise velocity fluctuations near the wall. (a) Data of Kyriakides *et al.*;[4] (b) present calculation, $Re_D = 385$.**

the leading edge first encounters an accelerating outer flow, and then a decelerating one. The corresponding acceleration parameter $K = (\nu/U_\infty)(dU_\infty/dx)$ (where $U_\infty$ is the velocity at the edge of the boundary layer) is initially large and positive. The region of large positive values of $K$ is, however, limited to the region $x/D \leq 1$ (Fig. 7); over most of the flat plate the acceleration parameter is below the value that may result in re-laminarization ($K \simeq 3 \times 10^{-6}$). In fact, for $x/D \geq 22$ the boundary layer is subjected to a mild adverse pressure gradient that is expected to favor transition to turbulence.

The streamwise development of several statistical quantities is shown in Fig. 8. The skin friction coefficient $C_f$ (Fig. 8a) from both calculations is very close to the value corresponding to the Blasius boundary layer. In the high Reynolds-number case we observe a significant increase of $C_f$ (towards the end of the computational domain); this issue will be discussed further below. The Reynolds number based on the momentum thickness, $Re_\theta$, is shown in Fig. 8b. For both calculations $Re_\theta$ remains very low. As mentioned before, the $Re_\theta$ values achieved in the $Re_D = 385$ case are unquestionably below the minimum values at which self-sustained turbulence is typically observed in flat-plate boundary layers. The $Re_\theta$ values from the high Reynolds-number calculation towards the end of the computational domain are perhaps marginal in this regard.

The power spectra of the streamwise velocity at $z/D = 0.15$ are compared in Fig. 9 with the experimental data of Kyriakides *et al.*[4] The experimental data was taken from Fig. 7 of the paper cited, which did not specify the distance from the wall at which the data was measured, nor the scale of the ordinate; the frequency has been rescaled to yield a dimensionless Strouhal number. Our calculations are in general agreement with the experimental observations; the shedding frequency is 0.22 (in the experiment a value of 0.21 was observed) and we observe a filling-up of the spectrum at both lower and higher frequencies with distance downstream of the cylinder. We do not observe, however, the harmonic peak measured in the experiment at $St = 0.42$. It is unclear whether this discrepancy is due to experimental or numerical errors, to insufficient sample convergence in the DNS, or to a difference in the location of the measurements.

Kyriakides *et al.*[4] observed that time-traces of the velocity at this height had a sinusoidal behavior up to $x/D \simeq 7.3$ and 2.7 for the low and high Reynolds-number, respectively; they identified transition with the loss of the sinusoidal behavior. The time histories of the velocity fluctuations (not shown) show depar-

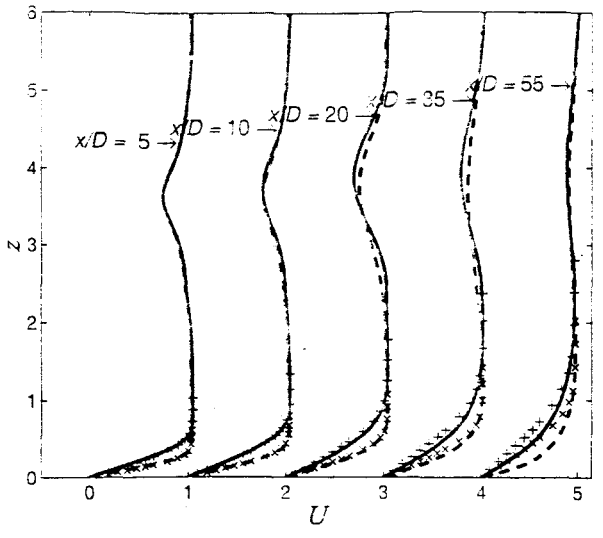


**Fig. 10 Mean velocity profiles at various locations. ——— $Re_D = 385$; --- $Re_D = 1,155$; × Blasius profile. Each profile is shifted by 1 unit for clarity.**

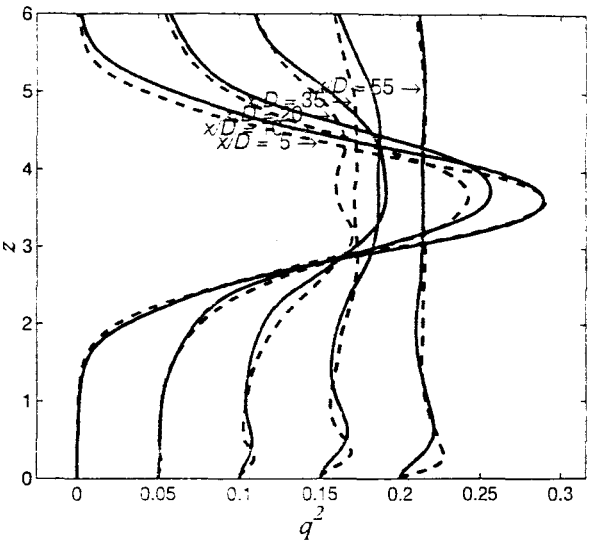


**Fig. 11 Profiles of $q^2$ at various locations. ——— $Re_D = 385$; --- $Re_D = 1,155$. Each profile is shifted by 0.05 units for clarity.**

ture from the sinusoidal behavior at similar locations. We believe, however, that a quantitative definition of the onset of transition is more desirable than the subjective one adopted by Kyriakides *et al.*[4] One possibility is to define the location of the transition point in terms of some threshold value of the turbulent fluctuations. Figure 8c shows the developments of the peak $\langle u'u' \rangle$ and $\langle v'v' \rangle$ Reynolds stresses, normalized by the local wall stress $\tau_w$. The streamwise Reynolds stresses reach values comparable to those expected in turbulent flows in the $Re_D = 1,155$ case, while they remain at about half of this level when $Re_D = 385$.

An important measure of transition is the onset of three-dimensionality. We observe that the spanwise Reynolds stress $\langle v'v' \rangle$ begins growing earlier for $Re_D = 385$ than for $Re_D = 1,155$. This is a consequence of the faster spreading of the cylinder wake at the low Reynolds-number. It will be shown later that the first onset of three-dimensionality in the boundary layer is caused by the passage of the vortices shed in the wake of the cylinder. The onset of three-dimensionality in the boundary layer is very well correlated with the onset of three-dimensionality in the wake.

Figures 10 and 11 show the profiles of the mean velocity and $q^2$ at several locations downstream of the cylinder. We observe a clear separation between the boundary layer and the wake near the leading edge, which disappears as one moves downstream. Up to $x/D = 20$ the velocity profiles agree very well with the Blasius solution at both Reynolds numbers. In the low Reynolds-number case we observe a mild growth of fluctuations in the boundary layer (evidenced both by the streamwise development of $\langle u'u' \rangle$, Fig. 8, and by the profiles of $q^2$, Fig. 11). These fluctuations, however, appear to be due entirely to the advection caused by the vortices shed by the cylinder, which, as they are

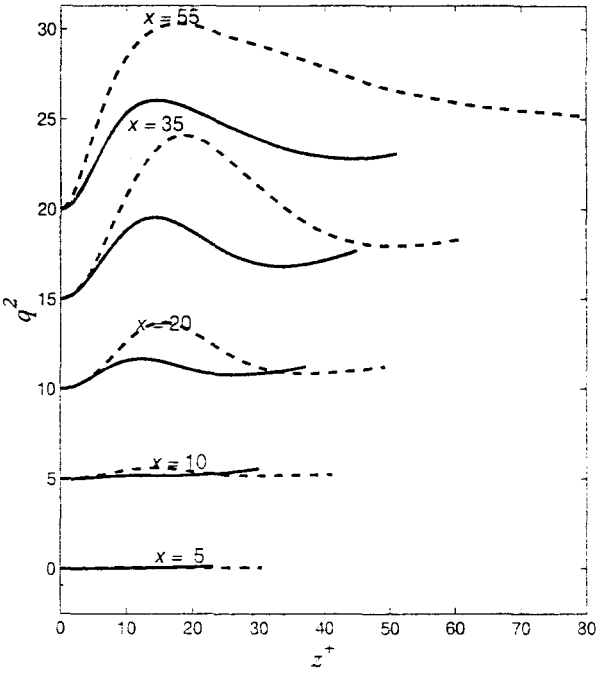


**Fig. 12 Profiles of $q^2$ in wall units at various locations. ——— $Re_D = 385$; --- $Re_D = 1,155$. Each profile is shifted by 5 units for clarity.**

convected downstream, induce ejections of low-speed fluid from the near-wall region. These velocity fluctuations, in fact, do not result in the levels of Reynolds shear stress $\langle u'w' \rangle$ typical of the turbulent flat-plate boundary layer (see below).

The high-Reynolds-number calculation shows a different behavior. Significant differences appear in the velocity profile at the downstream locations. At the last location shown ($x/D = 55$), $Re_x \simeq 58,000$ and

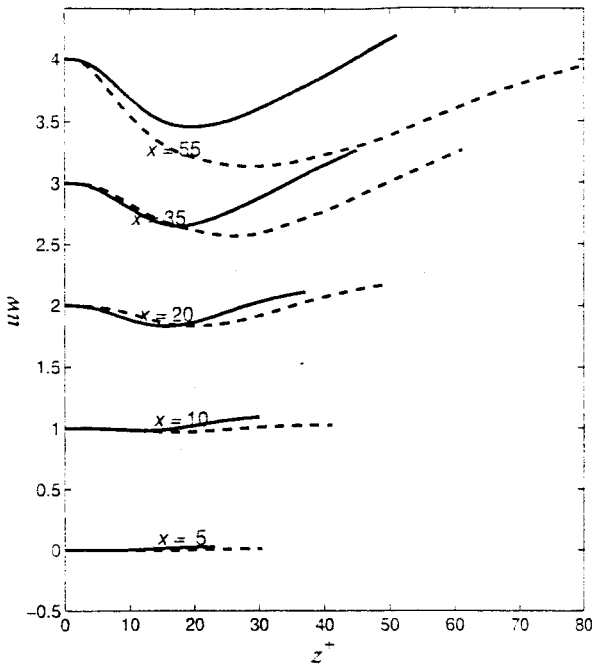


**Fig. 13 Profiles of $\langle u'w' \rangle$ in wall units at various locations. ——— $Re_D = 385$; --- $Re_D = 1,155$. Each profile is shifted by 1 unit for clarity.**

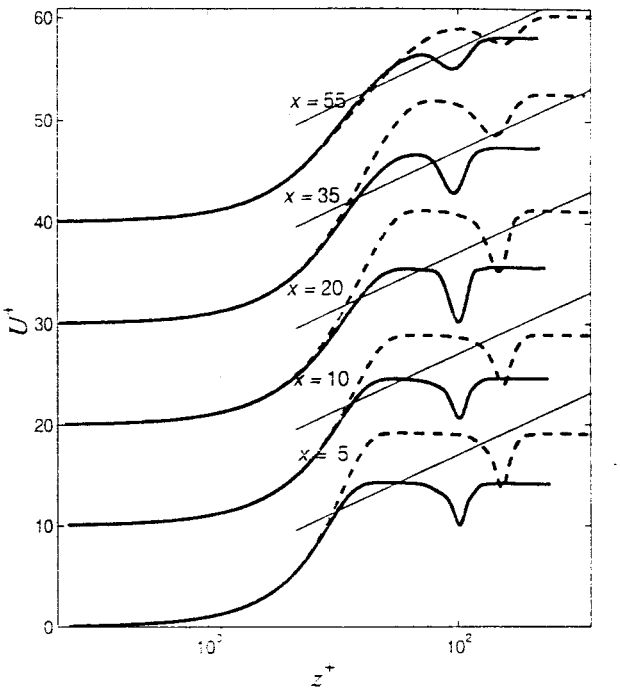


**Fig. 14 Mean velocity profiles in wall units at various locations. ——— $Re_D = 385$; --- $Re_D = 1,155$. Each profile is shifted by 10 units for clarity.**

$Re_{\delta^*} \simeq 340$. Although the flow has not achieved a fully developed turbulent state yet, there are several indications that transition to turbulence is taking place. The turbulent kinetic energy (Fig. 11), for instance, shows a near-wall peak that is increasing and moving towards the wall. The value of this peak and its location in wall units are those expected in a turbulent flat-plate boundary layer (Fig. 12). The Reynolds shear stress $\langle u'w' \rangle$ (Fig. 13) exhibits a similar behavior: its peak value and distribution for the high-Reynolds-number case are similar to those expected in turbulent flat-plate flows, while in the $Re_D = 385$ case the peak is significantly lower.

The Reynolds stresses appear to move towards a turbulent state more rapidly than the mean velocity profile; the shape factor $H = \delta^*/\theta$ remains close to the laminar value of 2.6 throughout the computational domain, and the mean velocity profile has not achieved a logarithmic profile by the end of the computational domain (Fig. 14). However, significant levels of turbulent fluctuations (r.m.s. levels between 1 and 10% of the freestream velocity) are observed within the boundary layer. At the downstream stations, the freestream turbulence at the edge of the boundary layer is very significant, between 3 and 5% of the velocity at the boundary-layer edge (for the low and high-Reynolds number cases, respectively), levels that are able to trigger bypass transition in boundary layers. Computations that use a longer domain should be carried out to determine the exact route to turbulence in the present configuration.

Figures 15 and 16 show instantaneous contours of the streamwise velocity fluctuations, and iso-surfaces of the second invariant of the velocity gradient tensor,

$$Q = -\frac{1}{2}\frac{\partial u_i}{\partial x_j}\frac{\partial u_j}{\partial x_i} = -\frac{1}{2}\left(S_{ij}S_{ij} - \Omega_{ij}\Omega_{ij}\right), \quad (5)$$

where $S_{ij}$ is the strain-rate and $\Omega_{ij}$ the rotation-rate tensor. In regions where $Q > 0$, the vorticity is due to rotational motions, rather than to shear.

In the low-Reynolds-number case (Fig. 15) the cylinder wake is very well-defined; staggered rows of quasi-2D vortices are shed, which are joined by clearly observable rib vortices. Three-dimensionalities quickly develop. There is a high correlation between the appearance of three-dimensionalities in the rollers, and the appearance of low- and high-speed streaks in the boundary layer (a very clear example can be observed around $x/D = 20$). This feature is connected to the increase of the spanwise Reynolds stress $\langle v'v' \rangle$ mentioned above. These streaks are convected with the freestream velocity, confirming the observation that they are induced by the outer flow: in turbulent flows, the typical near-wall streaks, which are generated in the inner layer, are convected at speeds that are 60–70% of the freestream velocity.

Another effect of the shed vortices on the near-wall region can be observed in Fig. 15c. Corresponding to the vortex street, one can observe alternating regions of high- and low-speed fluctuations, due to the advection from the upper and lower rows of vortices, respectively. These regions correspond to Q2 and Q4

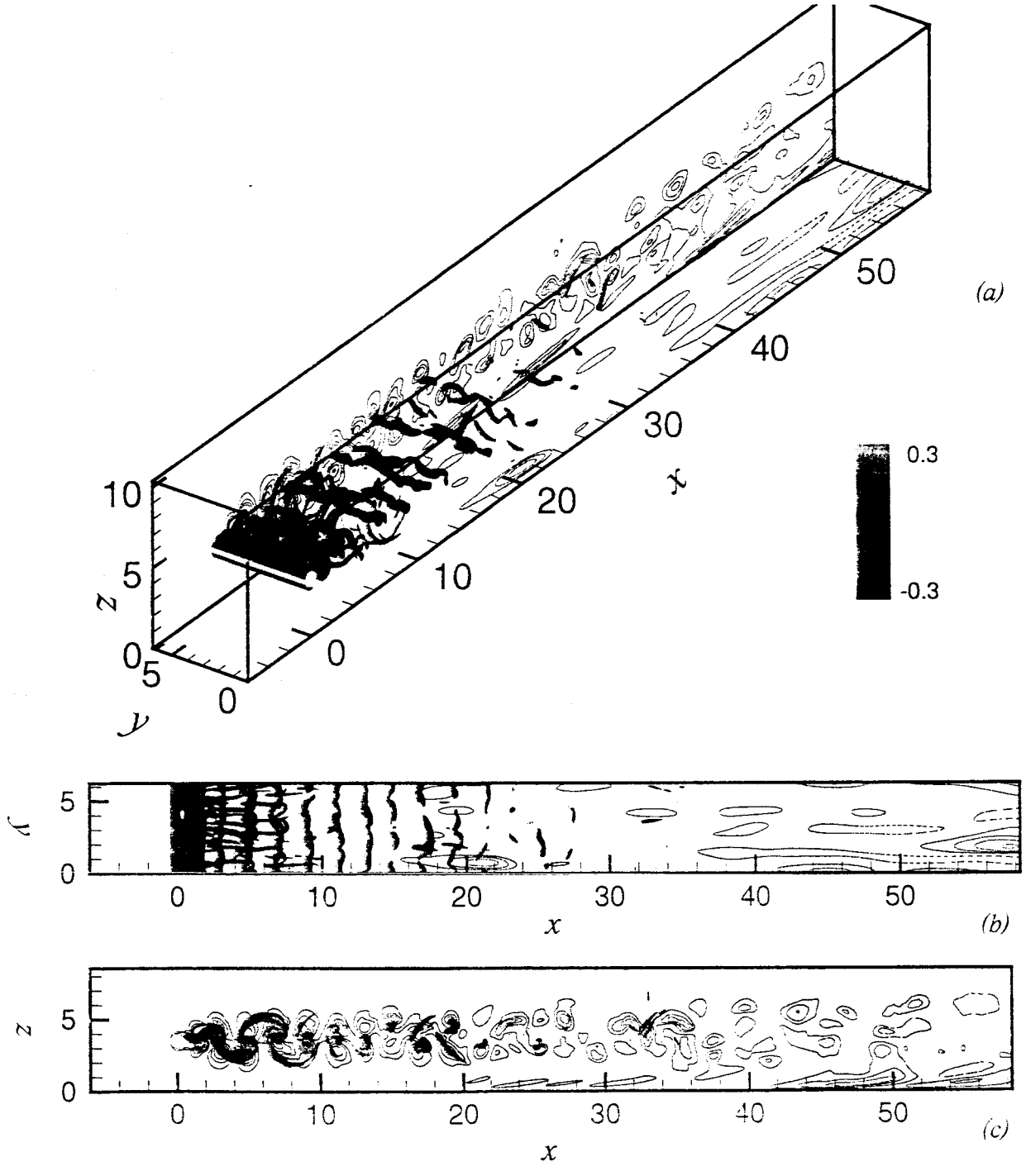


**Fig. 15** Isosurfaces of $Q$, and contours of the streamwise velocity fluctuations in a $xz-$plane and in the $z/D = 0.2$ plane. $Re_D = 385$. (a) Prospective view; (b) top view; (c) side view.

events,[20] and are responsible for regions of significant correlation $u'w'$. As the rollers become weaker, no new streaks are generated, and the flow does not appear to evolve into a fully turbulent state, the main disturbances being due to the streaks that are convected downstream, and weaken progressively.

At the high Reynolds-number (Fig. 16) a somewhat different picture emerges. Smaller-scale vortices can be observed in the wake, consistent with the increased Reynolds number. Also, the wake breaks down more rapidly. Well-defined rollers and rib vortices can, nonetheless, be observed. Some low-speed regions in the boundary layer can still be observed, corresponding to the onset of three-dimensionality in the rollers; unlike the low-Reynolds-number case, however, these streaks do not weaken significantly as they are convected downstream. The decreased viscous dissipation due to the increased Reynolds number certainly plays a role in this, but a self-sustaining turbulence generation cycle may also be beginning to appear. This conjecture is supported by the appearance of quasi-streamwise vortices in the near-wall region for $x/D > 50$.

## Conclusions

The work presented in this paper had a two-fold objective, namely, to establish the accuracy of the numerical code for wake-boundary-layer interaction problems and to clarify unanswered questions regarding prior experiments[4] related to such interactions. We believe that both of these goals have been nearly met through the work described here. In addition to code validation for building-block problems involving the isolated problems of cylinder wake and bypass transition in a flat-plate boundary layer, we have carried out large-eddy and direct simulations to understand the details of the strong interaction between a cylinder wake and a flat-plate boundary layer at two Reynolds numbers ($Re_D = 385$ and 1,155) selected from the low-$Re_D$ range in the experiment, for which transition was apparently observed.

We observe a region in which the cylinder wake perturbs the boundary layer by advecting low-speed fluid from the wall into the outer region, and high-speed fluid from the core towards the wall, as rollers of alternating rotation are convected above the boundary layer. Three-dimensional disturbances appear in the boundary layer in correspondence to kinks in the spanwise rollers. The appearance of streamwise vorticity in the wake is visually well-correlated with the presence of low- and high-speed streaks near the wall. This, and the fact that these streaks are convected downstream at the freestream velocity (rather than a convection velocity typical of near-wall phenomena) indicate that the perturbations in the boundary layer are forced from the outside, and not generated within the boundary layer itself. As the wake decays, the advection effect becomes less significant, but the wake generates high levels of freestream turbulence, that are expected to affect the flow downstream. In the low-Reynolds-number case the flow tends towards a more quiescent state towards the end of the computational domain and the statistics never reach turbulent levels. In the high-Reynolds-number case, on the other hand, the appearance of coherent, quasi-streamwise vortices is observed, which might be the prelude to the establishment of a self-generating cycle of sweeps and ejections. This was supported by the establishmnent of Reynolds-stress levels comparable to those observed in turbulent flows.

While some features of the computed flow fields are in satisfactory agreement with the measured data, the simulations indicate that transition does not really take place at the lower Reynolds number: the boundary layer is simply buffeted by the unsteady Kármán vortex street shed by the cylinder. For $Re_D = 385$ the fluctuations generated in this manner cannot be self-sustained due to low-Reynolds-number effects, and the boundary-layer flow does not transition to turbulence. We believe that the cause behind the discrepancy between the observations of Kyriakides *et al.*[4] and the above results is to be found in an unsatisfactory criterion for transition detection in the experiment, and in the lack of sufficiently detailed measurements of the type particularly required for transition studies. In contrast, in the higher Reynolds-number case, boundary-layer fluctuations persist even after the wake has decayed. This can be attributed, in part, to the spatial growth of the boundary layer during the interaction, which brings the $Re_\theta$ values closer to the typical range of minimum critical Reynolds numbers required for self-sustained turbulence in zero-pressure-gradient flows; some evidence could be observed that a self-sustaining turbulence generation cycle was beginning to be established.

Near-term extensions to this work will involve additional simulations to clarify the flow behavior downstream of the present domain. We also plan to investigate the possibility of higher-$Re$ simulations, which will also allow the present study of strong wake interactions to be extended to weak interactions. It will be interesting to find out the extent of similarities between the weak interactions and the familiar case of bypass transition due to moderate levels of free-stream turbulence.

## Acknowledgments

The first, third and fourth authors acknowledge the financial support of the NASA Langley Research Center, under Grant NAG12285.

## References

[1]Meredith, P. 1993 *AGARD CP-515*, 19.1.

[2]Squire L. C. 1989 *Prog. Aerospace Sci.* **26**, 261–288.

[3]Zhou, M.D., and Squire, L.C. 1985 *J. Aeronaut.* **89**, 72.

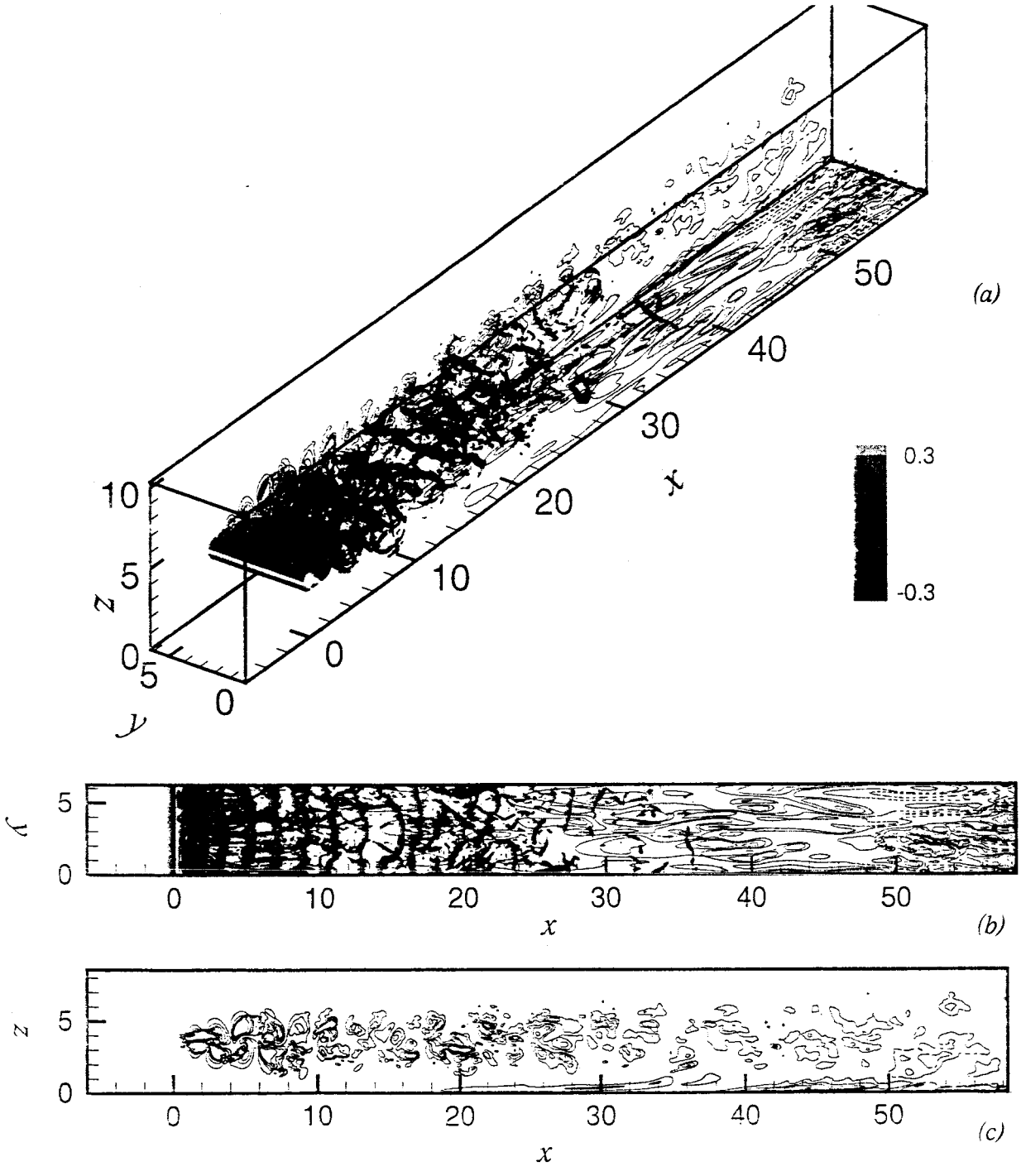


**Fig. 16 Isosurfaces of $Q$, and contours of the streamwise velocity fluctuations in a $xz-$plane and in the $z/D = 0.2$ plane. $Re_D = 1,155$.**

[4]Kyriakides N.K., Kastrinakis, E.G., Nychas, S.G., Goulas, A. 1996 *Proc. Inst. Mech. Eng.* **210**, 167.
[5]Kyriakides N.K., Kastrinakis, E.G., Nychas, S.G., Goulas, A. 1999 *AIAA J* **37**, 1197.
[6]Kyriakides N.K., Kastrinakis, E.G., Nychas, S.G., Goulas, A. 1999 *Eur J. Mech. B-Fluid* **18**, 1049.
[7]Chorin, A. J. 1968 *Math. Comput.* **22**, 745.
[8]Kim, J. and Moin, P. 1985 *J. Comput. Phys.* **59** 308.
[9]Meneveau, C., Lund, T. S., and Cabot, W. H. 1996 *J. Fluid Mech.* **319** 353–385.
[10]Mohd-Yusof, J. 1997 in *CTR Annu. Res. Briefs 1997*, NASA Ames/Stanford University, 317.
[11]Fadlun, E.A., Verzicco, R., Orlandi, P., Mohd-Yusof, J. 2000 *J. Comput. Phys.* **161** 35.
[12]Verzicco, R., Mohd-Yusof, J., Orlandi, P., Haworth, D. 2000 *AIAA J.* **38** 427.
[13]Balaras, E. 2002 Submitted to *Comput. and Fluids.*
[14]Balaras, E., Benocci, C., and Piomelli, U. 1995 *Theoret. Comput. Fluid Dyn.* **7** 207.
[15]Balaras, E., Piomelli, U., and Wallace, J.M. 2001 *J. Fluid Mech.*, **446**, 1.
[16]Piomelli, U., Balaras, E., & Pascarelli, A. 2000 *J. Turbulence* **1**, 001.
[17]Orlanski, I. 1976 *J. Comput. Phys.* **21**, 251.
[18]Voke, P., and Yang, Z. 1995 *Phys. Fluids* **7**, 2256.
[19]Roach, P.E., and Brierley, D.H. 1992 In *Numerical Simulation of unsteady flows and transition to turbulence*, O. Pironneau, W. Rodi, I.L. Rhyming, A.M. Savill and T.V. Truong, eds. Cambridge, 318.
[20]Wallace, J.M., Brodkey, R.S., and Eckelman, H 1972 *J. Fluid Mech.* **54**, 39.